



# Method for Rapid Modeling of Distortion in Laser Powder Bed Fusion Metal Additive Manufacturing Parts

J.V. Gordon, J. Pauza, A. Choi, M. Farfel, M. Bennett, R. Deering, B. Griffith, K. Johnson, Y.J. Zhang, A. Deal, and A.D. Rollett

Submitted: 19 January 2021 / Revised: 13 July 2021 / Accepted: 15 August 2021

The simulation and modeling of part-level distortion and residual stress in diverse metal additive manufacturing (AM) geometries has great potential to enable the rapid adoption of this technology in engineering design. Moreover, the use of additive manufacturing component libraries (CLs) offer a computationally efficient means of quantifying these part-level defects resultant from AM processing. We report on how the individual simulations of simple shapes, potential entries in a CL, can be superimposed to provide an indication of distortion and residual stresses in complex geometries. Laser powder bed fusion AM was used to construct test geometries of varied shapes and their combinations in the form of CLs in an effort to characterize location-dependent and feature-dependent distortion distributions. Blue light scanning was used to experimentally measure 3D distortions in order to investigate the interaction between the component shapes and local boundary conditions. Overall, part-level distortions were highly dependent on test component geometry, local boundary conditions, and shape combination. Commercial finite element software was used to verify experimental trends and to make predictions of distortion. The use of CLs resulted in over 20 times savings in computational cost while reproducing overall trends in distortion for test geometry assemblies. Therefore, it is anticipated that the use of CLs for L-PBF AM geometries has demonstrated potential to facilitate efficient simulations of full component AM assemblies, thereby reducing the need for costly trial-and-error-type experimental analysis.

**Keywords** additive manufacturing, blue light scanning, distortion, finite element analysis, residual stress, superposition principle

## 1. Introduction

It is well known that metal AM materials and components in the as-built condition experience thermal strains/stresses that develop during rapid solidification. While beneficial residual stresses may result in enhanced material strength and fatigue lifetimes in AM materials (Ref 1), the redistribution of residual stresses from the removal of parts from the baseplate can lead to non-trivial distortions, particularly for thin features (Ref 2-4). This behavior is highly undesirable for structural components

This invited article is part of a special topical focus in the Journal of Materials Engineering and Performance on Additive Manufacturing. The issue was organized by Dr. William Frazier, Pilgrim Consulting, LLC; Mr. Rick Russell, NASA; Dr. Yan Lu, NIST; Dr. Brandon D. Ribic, America Makes; and Caroline Vail, NSWC Carderock.

**J.V. Gordon**, Department of Materials Science & Engineering, Carnegie Mellon University, Pittsburgh, PA 15213; and Department of Mechanical Engineering, University of Michigan, Ann Arbor 48109; **J. Pauza**, **A. Choi**, **M. Farfel**, and **A.D. Rollett**, Department of Materials Science & Engineering, Carnegie Mellon University, Pittsburgh, PA 15213; **M. Bennett** and **Y.J. Zhang**, Department of Mechanical Engineering, Carnegie Mellon University, Pittsburgh, PA 15213; **R. Deering**, **B. Griffith**, and **A. Deal**, Kansas City National Security Campus, Kansas City, MO 64147; **K. Johnson**, Sandia National Laboratory, Albuquerque, New Mexico, NM 87185. Contact e-mails: jerardvg@umich.edu and rollett@andrew.cmu.edu.

and assemblies that must meet stringent requirements in tolerances. As such, many studies have focused on characterizing residual stress and distortion as a function of part geometry and processing variable selections. Kruth et al. (Ref 2) developed a rapid analysis tool involving bridge-shaped (arch) geometries that qualitatively assesses thermal stresses as a function of scan strategy and laser parameters settings. Two main findings were discovered: (1) changes which reduce temperature gradients, e.g., short scan vectors and preheating of the base plate, reduce the thermal stresses and, (2) thermal stresses in a particular direction can be reduced by optimal choice of the orientation of scan vectors. Wu et al. (Ref 3) performed a parametric study on the effects of laser scan strategy, power, speed, and build direction of residual stress distributions within AM 316L builds of L-shaped and prism-shaped geometries. Overall, decreased residual stresses were obtained by decreasing scan island size, increasing island to wall rotation to 45°, and increasing applied energy per unit length (laser power/speed). Comparatively, L-shaped geometries possessed a maximum compressive residual stress of approximately 300 MPa at the center and tensile residual stress of approximately 500 MPa at the edges with maximum displacement of 31 μm. For both horizontal and vertical prisms, in-plane tensile residual strains measured via neutron diffraction increased with proximity to the top surface of the AM parts causing them to deform spherically with the edges “peeling up”. This was attributed to constraint against in-plane shrinkage imposed by sub-surface layers coupled with reheating effects of the sub-surface layers. Follow-on studies by Hodge et al. (Ref 5), Ghasri-Khouzani et al. (Ref 6), and Simson et al. (Ref 7) supported those findings of large tensile residual stresses near the edges and tops of AM parts greater than 400 MPa. Importantly, it was discovered in (Ref 6) that after the removal of AM parts from the build plate and support

structures, the magnitude of the in-plane residual stresses decreased by as much as 330 MPa. However, this stress relaxation was accompanied by part distortion as measured with a coordinate measuring machine (CMM), with higher distortions for the disk-shaped geometries with smaller diameters and heights (Ref 4).

In an effort to minimize costly trial-and-error-type experimental analysis, predictive models for residual stress and distortion in metal AM builds have been employed in works such as Neugebauer et al. (Ref 4), Hodge et al. (Ref 5), Mukherjee et al. (Ref 8), Li et al. (Ref 9), Williams et al. (Ref 10), Strantza et al. (Ref 11), and Ganeriwala et al. (Ref 12). Notably, Hodge verified residual stress within L-shaped and prism-shaped geometries using a massively parallel high-fidelity implicit finite element analysis (FEA) code. Overall, the model supported the experimental findings and showed similar magnitudes of residual stresses, although local discrepancies were also discovered. These discrepancies were likely due in part to processing of the experimental data and partly to the choice of certain material parameters in the model; similar studies utilizing commercial FEA software (Ref 4, 8-10) have also shown this for simple geometries such as bridges, disk shapes, and cantilever beam geometries. However, while the high-fidelity and commercial FEA tools previously mentioned showed good agreement with experimental results, they also require significant computational resources and may not be able to perform rapid predictions of more complex AM geometries. This lack of rapid prediction that allows the user to avoid distortion problems is a significant bottleneck in the evaluation of potential metal AM components for engineering applications. Thus, in order to rapidly analyze AM component assemblies, we explore the possibility of superimposing the results of previously simulated component libraries (CL) to screen the deformation behavior of more complex geometries. Residual strains (stresses) are typically taken to be an elastic (linear) quantity; furthermore, typical analysis methods such as neutron diffraction utilize this feature to determine residual stress from crystal lattice strains (Ref 6, 13, 14). Therefore, the principle of superposition is potentially viable to analyze residual stresses and residual strains (i.e., distortions) resultant from AM processing methods. First, metal AM parts are geometrically decomposed into “component libraries” (CLs) of simple shapes, as shown in Fig. 1. In the example shown in Fig. 1, a “house” design is separated into three distinct components, namely: a triangular pyramid “house roof” and a rectangular “house body” (Fig. 1a). The roof and body components form a component library from which combined shapes (e.g., the full house geometry) or perhaps another geometry can be designed. Next, the distortion distributions are evaluated for each individual component using appropriate experimental techniques (Fig. 1b). Lastly, the distribution of distortions within each CL shape is then combined to form the final AM component (i.e., full house shape) through proper handling of location specific boundary conditions for each CL feature within a companion “superposition” model. This model is compared to the simulation of the full house geometry to determine the accuracy of the superposition simulation to capture distortions within the full geometry. Although this analysis is somewhat simplistic, it is anticipated that lessons learned from the use of superposition-based analysis will inform the applicability of quantitative analysis tools for prediction of distortions using FEA software for more complex geometries involving additional CL features.

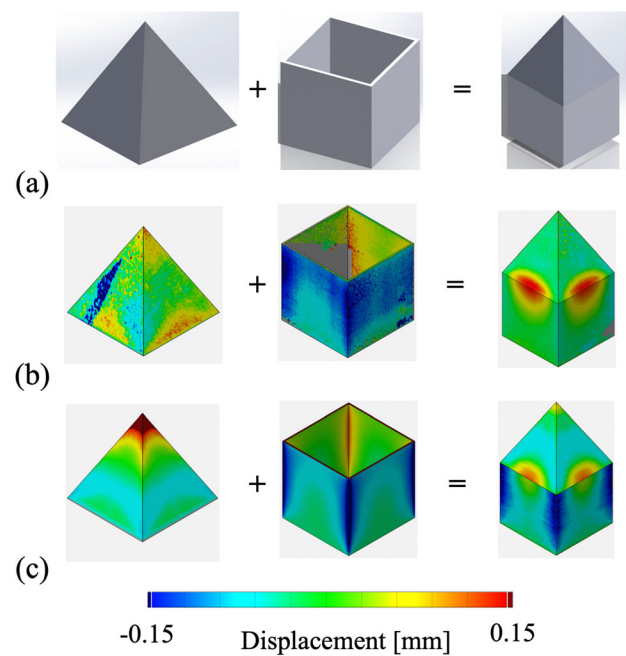


**Fig. 1** Example of CL methodology for metal AM. (a) The articles (e.g., house “roof” and “walls”) form a component “library”, by which adding them will give the desired full house geometry. (b) Experimental evaluation of distortions within individual CL articles, and the full geometry. This information is used to validate FEM simulations in (c), enabling rapid evaluation of suitability for diverse AM parts

Therefore, the primary goal of this study aims to characterize part distortions in metal AM components and assemblies in a rapid fashion by developing CLs of features and methods of combination. The primary objective is to characterize if measured distortion distributions within metal AM assemblies can be understood as the summation of these distributions for combined simple geometric shapes. These simple geometries can then be used to construct more complex components in a modular fashion. A second goal is to model the experimental results using computationally efficient commercial FEA simulations within simple geometries; these are then seeded as boundary conditions for simulations of larger component assemblies. In this way, complex geometries can be decomposed into a series of simplified shapes that can be individually simulated to provide a general indication of the distortion response for CL assemblies in a rapid manner. Ultimately, the goal of this study is to advance the capability for efficient prediction of additive manufacturing outcomes with a particular focus on distortion in laser powder bed fusion (LPBF) and 316L stainless steel as an exemplary material.

## 2. Materials and Methods

### 2.1 Process Settings and Sample Geometries for CL Fabrication

Pre-alloyed gas atomized 316L stainless steel powder was used to fabricate test components and component assemblies on an EOS® M290 laser powder bed additive manufacturing system. A standard processing parameter set was used for all

test components, including a Yb-fiber laser power of 195 W, scan velocity of 1083 mm/s, hatch spacing of 90  $\mu\text{m}$ , layer thickness of 20  $\mu\text{m}$ . A rotating scan pattern was applied, wherein the hatching direction was rotated by 67° between the consecutive layers. Builds on two M290 machines at different locations were undertaken in order to evaluate variations in distortion based on machine and feedstock choice. Negligible variations in printing, or observed distortion properties were observed between the two systems. This in itself provides some evidence that machine-to-machine variations need not be a major concern for properly setup systems that are actively maintained.

The list of component geometries and combined assemblies is given in Table 1. Test articles were combined to create “House” shaped geometries made up of four vertical walls and a four-sided pyramidal roof. The individual test article geometries were chosen for their simple shapes which could serve as a proof-of-concept and preliminary comparison between the superposition-based analysis, full FEA simulations, and blue light experimental data. Particularly, the “Walls” and “Roof” shaped test articles are prime candidates for CLs as they are common shapes which may be superimposed to create various AM components such as alternating honeycomb structures for light weighting or matrix designs within heat exchangers (Ref 15-17).

All components for blue light scanning measurement (Ref 18, 19) were evaluated using a GOM ATOS III (Triple Scan). The blue light scanning technology, also known as structured light scanning, was controlled via an MCXL computer numerical controller. When necessary a Magnaflux SKD-S2 developer was used to limit light reflection during scanning. Developer coating was estimated to be between 3 and 15  $\mu\text{m}$  in thickness. Components were scanned with a 170 mm measurement volume, with 10-20 scans executed for a 360° rotation with the sensor at an angle of 45° to the measurement piece. A secondary scanning rotation was executed as necessary if additional data was needed to be captured in the scan (resulting in data capturing approximately 40 scans in excess of 1 gigabyte of data). The measurement volume had an estimated performance accuracy of better than 25  $\mu\text{m}$ . Measurement sensor and program settings were established in ATOS Professional 2018, exposure was set via GOM’s automated exposure setting, with multiple exposures per measurement ranging between 60 and 320 milliseconds. Scan data were then operator reviewed for quality and post-processed to a mesh at the highest detail per the software. Mesh data was then compared against a reference CAD file.

## 2.2 Component Library-Based Simulation Approach

The AM simulation modules within the Ansys Mechanical (2020R2) Additive Workbench and Abaqus Simulia (2018HF5) commercial FEA software packages were used to simulate the build process for each of the test components and component assemblies that were scanned. While each software possessed different solvers, interfaces, and required inputs, every attempt was made to make the models as substantially similar as possible in order to validate the superposition approach through replication in two prominent, but independently developed codes. Within each package, two core “models” were used—the traditional AM thermo-mechanical simulation workflows and a custom superposition workflow. Unless otherwise mentioned, the models used software defaults.

**2.2.1 Abaqus FEA Software.** In more detail, Abaqus’s thermo-mechanical FEA simulation methodology is to first solve for transient heat flow which then provides a temperature history for a subsequent structural analysis (Ref 20). The heat transfer utilizes a full laser path which treats the laser as a point source and calculates the amount of energy deposited by solving for the amount of time this point source spends in each element. This laser path was made with generic L-PBF processing parameters for SS316L: 353 K build temp, 8 s recoater time, 50  $\mu\text{m}$  slice height, and a laser sequence consisting of a contour pass followed by a raster infill. The contour is a single pass 110 W laser with a speed of 200 mm/s and a diameter of 75  $\mu\text{m}$ . The infill is a traditional hatch pattern with a spacing of 110  $\mu\text{m}$  and a 67° rotation between layers utilizing a 200 W laser with a scan speed of 750 mm/s and a diameter of 75  $\mu\text{m}$ . This slice profile and path were then imported into the FEA analysis. While these parameters are not exactly identical to the physical build parameters, owing to the spatial and temporal discretization that are required to run a simulation in a reasonable time, the macroscale distortion results are weakly sensitive to specific laser path changes. Each AM simulation—walls, roof, and full house had identical simulation setups; the only difference was the geometry being simulated. Each simulation included a 100 mm  $\times$  100 mm  $\times$  10 mm baseplate which was meshed with 3 mm C3D8R linear hex elements. Parts were meshed with the same linear hex elements except the seed size used was 0.33 mm in order to achieve three elements through the 1 mm wall thickness. Tied contact was defined between the top of the baseplate and the bottom of the part. The material used for both the baseplate and the part was a fully temperature dependent elastic–plastic stainless steel model with parameters identical to Ansys’s AM library SS316L material. Adaptive time-stepping was used with an initial and maximum timestep of 32.5 s (roughly the time to activate a full mesh

**Table 1 Test component geometries and assemblies within CL**

Number	Test Article	Height	Combined Articles
1	51 mm House Walls	25.5 mm	...
2	51 mm House Roof	25.5 mm	...
3	51 mm House Assembly	51 mm	1 + 2
4	102 mm House Walls	51 mm	...
5	102 mm House Roof	51 mm	...
6	102 mm House Assembly	102 mm	4 + 5

layer). For the transient heat flow simulation, the absorption coefficient of the laser was 0.45 and the initial temperature of the entire model was 353 K. The only other boundary condition (BC) applied was a radiation and convection boundary condition on the evolving exterior surface of the part. Each condition had a reference/enclosure temperature of 353 K and the radiation had an emissivity of 0.25 while the convection coefficient was defined to be 18 W/K-m<sup>2</sup>. The structural simulation fully constrained all degrees of freedom on the bottom of the baseplate. It mapped the temperature history from the first analysis and assumed that the part started from 1000 K (this is the temperature that thermal strain was calculated from and, above this temperature, the material was assumed to be stress-free).

**2.2.2 Ansys FEA Software.** The Ansys simulation workflow is a similar thermo-mechanical, layer-by-layer analysis as Abaqus, but instead of resolving the laser path, a full mesh layer is activated at a time from melt which subsequently cools for the approximate time it took to build those layers. This is also known as the “lumped layer” approach. This temperature history is then similarly fed into a structural analysis where displacements and residual stress from the induced thermal strain are solved. Since the Ansys model models the same set of physics as Abaqus, the two share many of the same boundary conditions. Where applicable, the identical values were used as identified within the Abaqus description above (Sect. 2.2.1). The simulation was set up through the “Additive Wizard” which provided a step-by-step guide and automatically assigned all of the boundary conditions described by the Abaqus model. The only BC not assigned was radiation. By default, Ansys does not generate a radiation boundary condition so no radiation loss was captured. Additionally, it should be noted that Ansys activates elements at melt temperature rather than using a user-defined, stress-free temperature (1000 K in Abaqus). The main difference between the models (aside from the solvers and previously noted differences), came from the mesh. In Ansys, each mesh layer has to be exactly uniform in height since each mesh activation turns on an entire layer at a given point in time. Several meshing schemes were available including hex and tetrahedron. However, the hexahedral (hex) meshing generates a non-conformal voxel mesh which only approximates the volume of the part. This leaves an artificial stair-step contour on the “Roof” of the house, as well as the potential to significantly alter the dimensions of the thin-walled shape depending on spacing of the voxel generation. Motivated by these concerns and to better match Abaqus’s conformal mesh, a layered tetrahedral (tet) mesh was used for all Ansys simulations. This layered tet mesh was given the same seed size (0.33 mm) as Abaqus and used quadratic elements.

**2.2.3 Superposition Approach.** For the superposition model within Abaqus, the end stress state of the individual parts was mapped onto the undistorted geometries of the “Roof” and “Walls” which were instantiated and positioned to form the “House.” The two base parts were treated as discrete entities in the superposition and the interface where the parts intersected were tied together via a tie constraint. The mapping was done via \*External Field, a sub option of \*Initial Conditions, TYPE = Stress and the full “S” variable was mapped for each individual part. Likewise, PE, PEEQ, and PEMAG were mapped using identical initial conditions of TYPE = Plastic Strain. Once the mapping was done, the whole structure was allowed to relax and resolve any remaining

residual stress over a single static structural step. The only BC was a fixed displacement on the base of the walls where the hypothetical superposition house part would still be affixed to the baseplate. Several superposition simulations using the nominal geometry (instead of the distorted) were run to allow for direct comparisons to Ansys results.

Likewise, for the superposition simulations in Ansys, a final structural analysis step was devised which took in the “solution” states of the previous component analyses and instanced those in the “model” of the new static structural step. APDL commands (“inistate”) were used to read in the variables needed to initialize the superposition simulation to the same end-state of the individual component’s AM simulation. When initializing, the plastic strain (“eppl”) and stress (“s”) were transferred to the new superposition simulation. The equilibrium state was then solved for in a two-step process. The first step was the two parts being instantiated with the appropriate residual stress state. During this step, a fixed displacement boundary condition was applied to base of the roof part (as if still attached to the baseplate). In the second step, this boundary condition was removed and tied contact was defined between the two pieces. They then reached an equilibrium with only a single fixed displacement BC at the base of the walls.

### 3. Results

#### 3.1 ANSYS CL and Superposition Results for the 51 mm Test Articles

Figure 2 compares the experimental blue light and Ansys FEA results for the 51 mm individual test components and assembly denoted in Table 1. The individual geometries for the Wall and Roof sections were approximately 25.5 mm in height, with the combined assembly of components (Walls + Roof) being approximately 51 mm in height (Fig. 2c). Overall, the simulated geometries show good agreement with the experimental results in terms of the trends and magnitude of distortion observed in blue light scans. Note that the axis of displacement is normal to the surface of each component. For the Wall components, inward deformation (visible as “sucking in” of the walls) is evident, which gradually increases with height. Interestingly, vertical Wall edges show slightly more inward movement than the faces. Localized distortion near the baseplate is evident in the Wall components, leading to a semicircular “sunrise” patterning. Although the simulation results capture the inward displacement near the Wall edges, the inward displacement of the Wall faces is under-predicted by the model (Fig. 2d). Furthermore, the semicircular “sunrise” patterning near the baseplate is also under-predicted. The individual Roof components show similar behavior to the Wall components; here, the localized strain near the baseplate is evident. One significant difference from the Wall components is the fact that blue light results do not display inward displacement of either the inward faces or corner edges for the Roof component. The simulation results predict inward displacement for the Roof edges although this is not evident in the blue light scans. The simulation also under-predicts deformation of the base (Fig. 2e) and shows more inward displacement in of the faces of the Roof than was observed in the experiments.

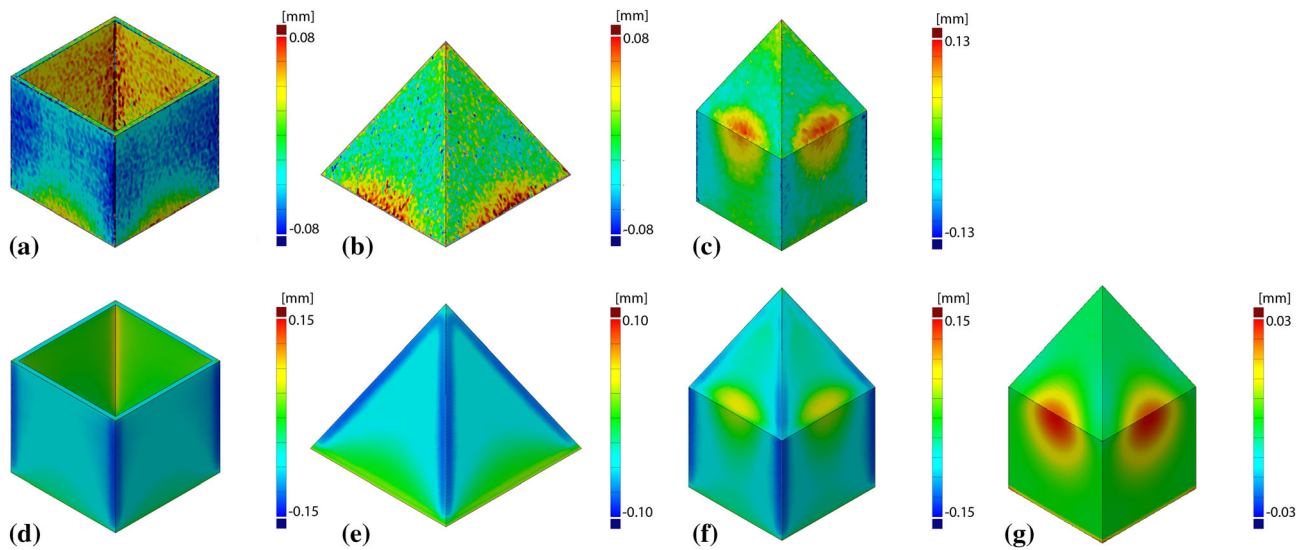


**Fig. 2** Comparison of experimental blue light results and comparison FEA of distortion (residual displacements) for 51 mm house shapes and assemblies. (a-c) denote experimental values, while (d-f) show model results. (g) is the 51mm Ansys superposition simulation. Note that each image was scaled to its own maximum deviation. The axis of displacement is normal to the surface of each component

**Table 2 Comparison of Ansys run times for the full model and superposition model of the 51 mm height test articles**

Simulation	Runtime, 8 CPUs
Walls	1.25 h
Roof	3.40 h
Full Simulation	5.60 h
Superposition	16 min

Figure 2(c), (f) compare the experimental and simulated results for the full assembly of features. Overall, good qualitative agreement between the blue light and model results were also observed here. The experimental results for the assembly walls show negligible inward displacement on both the faces and edges as compared to the component Wall geometries. However, the “target” or “bullseye” patterning near the wall/roof interface is clearly observed in both the blue light and simulation; here, the blue light shows higher localized displacements than the simulation. However, the roof /wall interface reproduces the high distortion values seen in experiments. As with the component features, the maximum magnitude of displacements is higher in the simulated features versus the experimental data, particularly for the edge features.

Next, the Ansys FEA superposition simulations were undertaken to make comparisons with the experimental blue light results and full assembly simulations. Figure 2(g) presents the superposition FEA simulation for the 51mm house geometry. Overall, the superposition shows good agreement, while also capturing the general trends seen in the experimental results. Noticeably, the superposition simulations were accomplished in a fraction of the compute time as compared with the full simulation (approximately 5 minutes versus > 6 hours) as shown in Table 2. Importantly, the superposition results show good agreement with the full simulation in reproducing the localized displacement near the wall and roof edges and the

wall/roof interface. However, the (slight) inward displacement at the corners of wall faces in the blue light and full simulation are not captured by the superposition simulation. Overall, the superposition method enables good qualitative agreement with approximately 23 times less compute time compared to the full simulation. As for the full simulation results, the superposition displacement magnitudes are smaller than the experimental values.

### 3.2 ANSYS CL and Superposition Results for the 102 mm Test Articles

The ability to scale-up the CL-based superposition predictions of part-level distortion was investigated for articles approximately  $2\times$  the geometric dimensions of geometries examined in Sect. 3.1. The 102 mm test articles consisted of a 102 mm house and the two corresponding wall/roof components each measuring 51 mm tall. Fig. 3 displays the blue light (Fig. 3a-c) and Ansys FEA simulation (Fig. 3d-f) for the individual wall and roof test articles as well of their full assembly. Similar trends as compared to the 51 mm test articles are observed, namely: (1) inward displacement at the corners for individual test components, (2) localized deformation near the baseplate for both Wall and Roof test articles, and (3) “sundial” patterning near the wall/roof interface in the full assembly. Importantly, the 102 mm test articles were found to possess higher amounts of net displacement, as compared to the 51 mm test articles (shown by the scale bars in Fig. 3(c), (d). This resulted in maximum displacements over 250 % higher in the full assembly for the 102 mm test articles than in the 51 mm test articles. Such a large increase in displacement is not trivial and confirms the recent findings that taller, thin-walled structures are more susceptible to deformation than the shorter ones (Ref 8).

Figure 3(g) illustrates the distortion results of the Ansys FEA superposition simulation for the 102 mm height test article. As with the smaller 51 mm test articles, the general trends of displacement are captured by the full and superposition simulations; however, the magnitudes of simulated

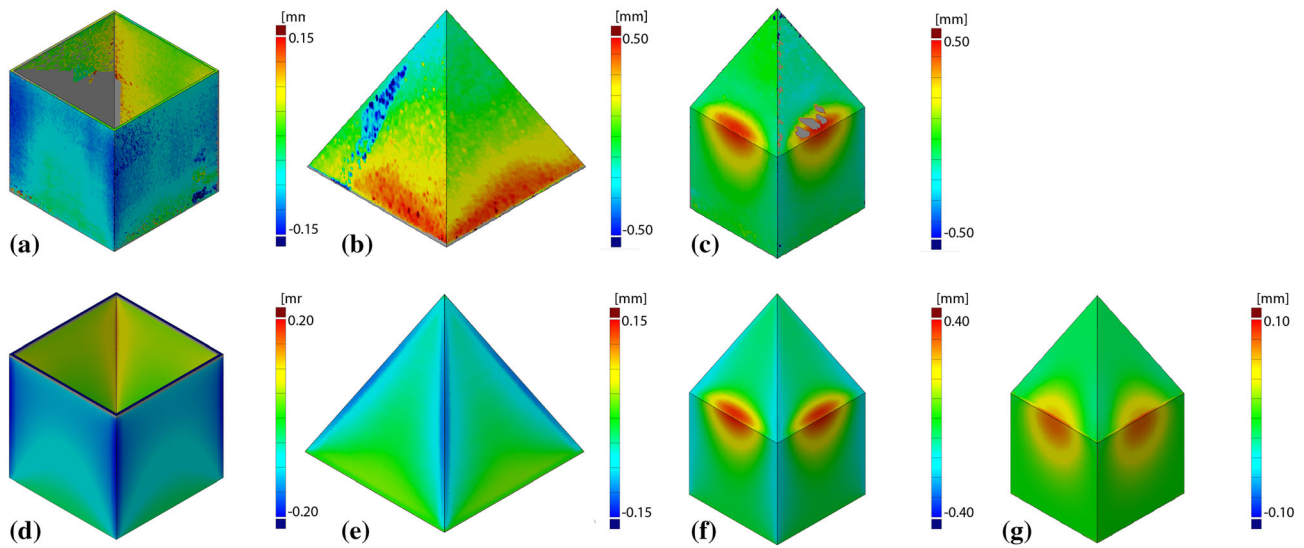


**Fig. 3** Comparison of experimental blue light results and Ansys predicted distortion (residual displacements) for 102 mm house shapes and assemblies. (a-c) denote experimental values, while (d-f) show model results. Again, each image is scaled to its respective maximum displacement

**Table 3 Comparison of simulation run times for the full model and superposition model of the 102 mm height test articles (Ansys)**

Simulation	Runtime, 36 CPUs
Walls	2.25 h
Roof	7.66 h
Full Simulation	116.25 h
Superposition	46 mins., 12 CPUs

distortions remain much lower than the experimental data. Importantly, the superposition simulation shows excellent qualitative agreement with the blue light for the Wall/Roof interface “sundial” deformation pattern. Both the full FEA simulation and the superposition approach fail to capture the large amount of distortion observed in the experimental build. Interestingly, the flaring out at the cap to body interface and the inward “sucking in” of the corners of the body section are not observed in the 102 mm assembly and are also not replicated in the simulations. Additionally, the full FEA simulation is able to capture the general shape of the distortion at the cap to body interface better than the superposition simulation. When comparing the 51 mm and 102 mm superposition approaches, the magnitude of the distortion trends in the same direction as the experimental blue light data. This illustrates that the modeling approach does correctly predict the trend of the distortion behavior over the shift in length scale. Lastly, a substantial savings in computational cost is observed when scaling to the larger 102 mm test articles. It should be noted that the superposition simulation leverages already run components and that each component has to be run exactly once before the results can be added to the library. For stand-alone or unique projects that require individual components to be simulated first, the process would be on the order of 10.5 hours if the individual component simulation time was considered (e.g., including the time for the Walls + Roof + Superposition

simulations in Table 3). In this case, the superposition simulations takes  $\sim 10.5$  hours to run as compared to the full simulation which takes approximately 116 (wall clock) hours. Therefore, even when including the time needed to simulate individual components, the superposition method results in a substantial time savings as compared to the full simulations for the 102 mm CL assemblies.

### 3.3 Comparison of Abaqus and Ansys CL and Superposition Results for the 102 mm Test Articles

The distortion of the 102 mm test articles was simulated using both Ansys and Abaqus FEA software in order to directly compare performance of superposition as implemented in both software packages. This included the simulation of the separated Roof and Wall geometries in addition to the full assembly and the superposition simulations. Figures 4 and 6 display the comparison of the Abaqus (Fig 6 a-c) and Ansys (Fig 4d-f) simulation results and the experimental blue light data (Fig 4a-c). Importantly, both software packages provide good qualitative agreement in distortion trends of the experimental data. However, the Abaqus results appear to better capture both the trend and magnitude of distortion near the interface between the part and the baseplate (Fig 6a-b). Overall the Abaqus simulated maximum distortions are lower than the experimental blue light maximum displacement values for the 102 mm test articles.

Figure 4 shows that the maximum distortions predicted for the individual components and full FEA simulation of the Ansys package (Fig. 3) is about twice that of the Abaqus package (Fig. 4). Some of this quantitative difference can likely be attributed to the temperature from which the packages begin calculating thermal strain. Abaqus has a user-defined value which is generally prescribed to be below the melt temperature whereas it is the latter that Ansys defaults to using. Furthermore, the Ansys simulations generally overpredict the measured displacements locally. This can be observed for the Ansys simulation of the wall (Fig. 3d) and roof (Fig. 3e) components. Here, the amount of inward displacements seen along the

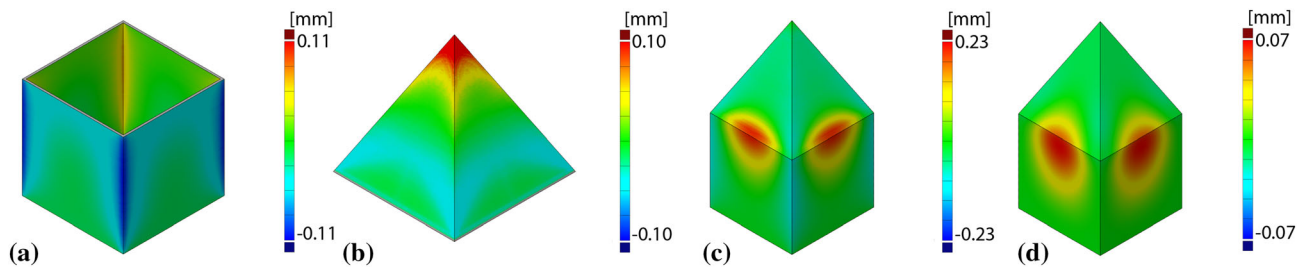


**Fig. 4** Comparison of Abaqus simulations of the distortion of the 102 mm test article geometries. (a) simulation of walls (b) simulation of cap (c) full house simulation (d) superposition simulation with nominal components for direct comparison to Ansys. Note the different scale bars for each geometry

corners of these shapes are overpredicted. Importantly, the highly localized distortion behavior is not observed in the experimental blue light data nor in the Abaqus simulations. Interestingly, the superposition simulation run in Ansys substantially under-predicts the magnitude of distortion (Fig. 3g). However, the shape of the distortion is very similar to the distortion seen in Fig. 3(c).

## 4. Discussion

### 4.1 Computational Savings and Accuracy of Superposition Analysis

As previously mentioned, the benefit of superposition is the potential speedup in computation time as compared to full simulations of part-scale AM builds. This is expected to enable the rapid assessment of multi-component AM structures based on a library of common geometric shapes. Since the traditional AM simulation relies on layer-by-layer activation of elements, an increase in build height results in more costly simulations via solving for a greater number of active degrees of freedom (DOF). Additionally, mesh height dictates the number of layer activations which means that the overall accuracy based on mesh refinement has a strong adverse effect on runtime as the mesh is refined in the build direction (Tables 2 and 3). Therefore, by simulating the two components individually, a similar qualitative result was obtained at a fraction of the computational time. The speedup in superposition analysis is evident in Tables 2 and 3. While the superposition analysis results in an exceptional savings of  $\sim 21$  times savings for the 51 mm assemblies, the 102 mm assemblies observe greater than 150 times savings assuming the CL entries existed already and could be leveraged. An example of this was clearly demonstrated via the Ansys runtimes of the 102 mm House. The runtime for the “Walls” was 2 hrs 16 min, the runtime for the “Roof” was 7 hrs 40 min; comparatively, the runtime for the full “House” was 116 hrs 25 min and the superposition was 46 minutes. Despite having the same seed size and total number of simulation layers, by dividing the model in half and simulating individual components, there is significant increase in computational speedup. By contrast, simulating each individual layer in a single build required several days. Therefore, the most beneficial property of superposition analysis applied to AM CLs is that similar qualitative profile of distortion can be obtained at a fraction of the time; This is particularly true for taller geometries, particularly ones possessing thin-walled

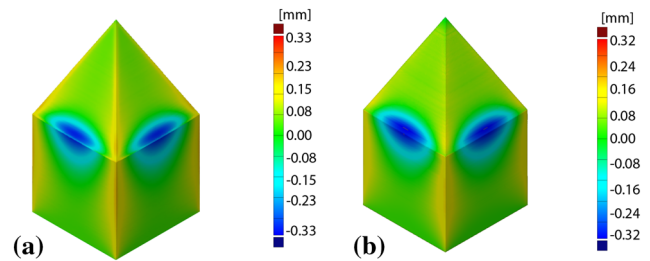


**Fig. 5** Superposition result plotted against the simulation results of the full house for Ansys (a) and Abaqus (b). Note: Abaqus results have been scaled by a factor of two so that Ansys and Abaqus results are comparable

features where distortion (as opposed to residual stress buildup) is a key defect structure effecting part performance (Ref 8).

Although extraordinary computational savings were enabled using the superposition analysis, it is important to understand classic speed-accuracy trade-off between the full simulations and superposition simulations in this study (Tables 2 and 3). Figure 5 shows a difference map between the distortion calculated in the full simulation of the 102 mm components against the superposition results for the Ansys and Abaqus simulations. The red color in Fig. 5 indicates areas where the superposition approach predicts less shrinkage, versus blue for more. Ideally, these two sets of results should line up everywhere; this would display a high accuracy (low error) for superposition versus the full simulation. It is important to recall that the maximum distortions within the 102 mm simulations for Ansys were 0.40 mm (full assembly) versus 0.10 mm (superposition); similar to the values for Abaqus of 0.23 mm (full assembly) versus 0.07 mm (superposition) for Abaqus (Figs. 3 and 4). Therefore, the Abaqus results of Fig. 5(a) have been scaled by a factor of two so that Ansys and Abaqus results are comparable. The difference map results in Fig. 5 shows good agreement for the superposition simulations versus the full house assembly in all areas away from the Wall/Roof or Wall/baseplate interfaces with a maximum discrepancy of approximately 0.32 mm for Abaqus and 0.33 mm for Ansys. However, most of the distortion shown by the difference maps for both Ansys and Abaqus are between approximately 0 and 0.150 mm away from the localized distortion patterns at the wall/roof interface. This means that for all areas away from these interfaces, the superposition analysis shows good agreement with full simulation; this is shown by the predominantly green and yellow coloring in Fig. 5(a-b). Therefore, to a first approximation, the superposition results show good accuracy when compared to the full assembly house simulations. A

probable reason for difference in magnitude between the Abaqus superposition results and full house simulations in Fig. 5 are due to the fact that we are only passing the stress state and plastic strain from simulated components onto the superimposed undistorted geometry in the Abaqus simulations. Furthermore, Fig. 5 only analyzes distortion in terms of a difference map showing absolute movements (which are relatively small); this may not be the best metric to compare part-level distortions. Therefore, further quantitative analysis is necessary to determine the accuracy of superposition method in reproducing distortion trends for CL features and assemblies.

#### 4.2 Quantitative Comparisons of Superposition Analysis

Although the superposition simulations captured general trends for both 51 mm and 102 mm height test articles and their assemblies with good accuracy, quantitative analysis is necessary to reach strong conclusions on the effectiveness of the proposed methods. Importantly, the accuracy of the superposition analysis can be further evaluated based on the ability to capture local trends within the blue light data. An example of this is the displacement variations along the test article midline walls, particularly near interfaces such as the baseplate and Roof/Wall (Fig. 6). In order to make robust conclusions for the effectiveness of superposition method in capturing specific trends of the experimental data, Fig. 6 presents qualitative comparisons in the form of displacement plots across a specific length of geometry for the blue light, Ansys, and Abaqus

simulated distortions. The simulated data in Fig. 6 were scaled and offset to account for the lower maximum displacements and part deflections of the simulations compared to the blue light data (Table 4). A comparison of the different test geometries and their associated scale and offset factors are given in Table 4.

The quantitative analysis of the individual components, full house assembly, and superposition are presented in Fig. 6. Overall, the simulated results for both FEA models compare favorably for both the wall and roof individual components with some deviation for the 102 mm Ansys wall and roof features; here, the Abaqus model appears to better conform to the shape of the displacement measured from the blue light scan than the Ansys simulations. The full house assemblies show excellent agreement with experimental data, particularly once shifted and scaled by appropriate factors (Table 4). Comparatively, the superposition simulations show good agreement in capturing the displacement trends observed in the measured blue light data. However, the superposition results require a maximum scale factor approximately 6 for the Abaqus 102 mm simulations, as compared to a scale factor of 2 for the Ansys 102 mm simulations. This reduced accuracy of the quantitative distortions is most likely due to our method of analysis which includes passing the final CL distortion to an undeformed superposition geometry and allowing the part to relax. In this way, the distortion trends of the part are captured, with the exception of those areas that have deformed sufficiently to relieve the majority of the stress in the CL articles (Section 2.2).

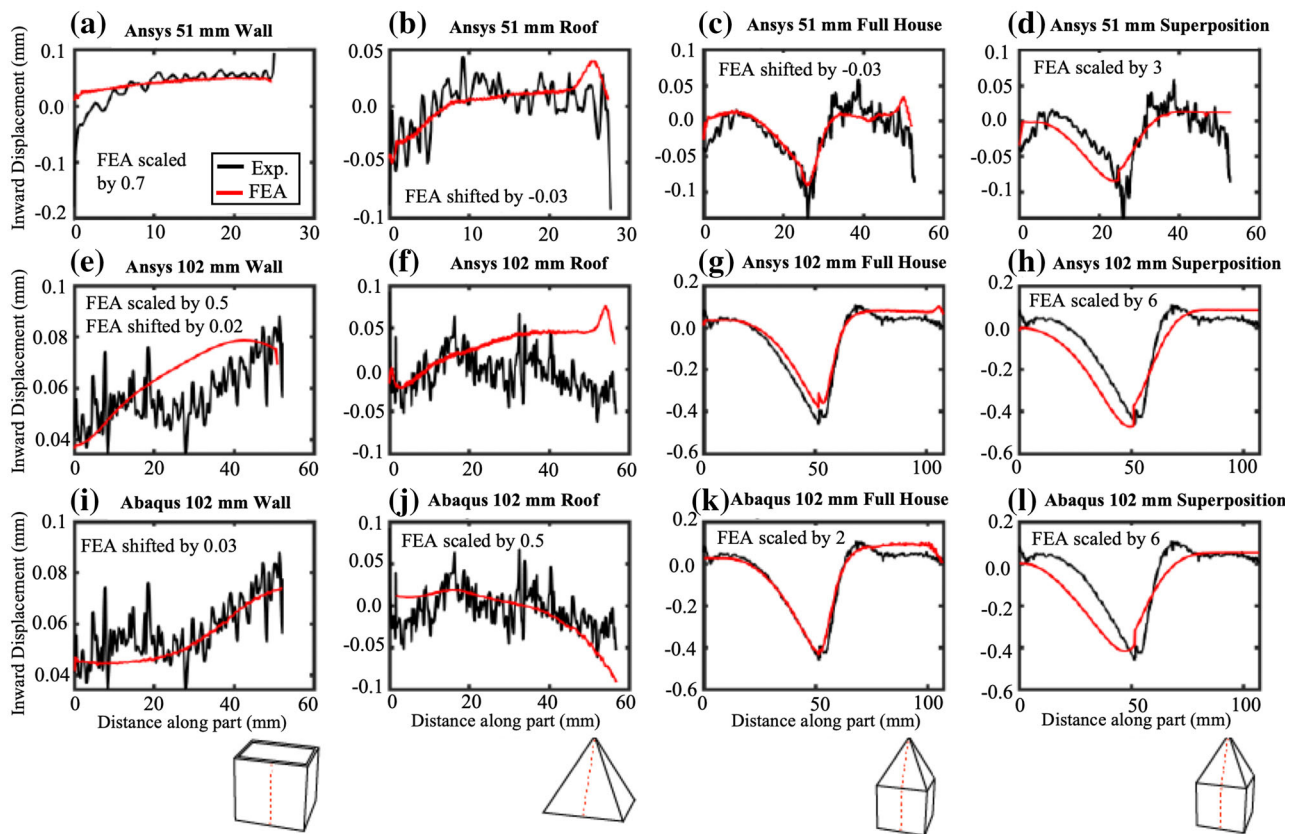


**Fig. 6** Cross-sectional quantitative comparison of experimental and Ansys simulated distortions for 51 mm (a-d) and 102 mm test articles (e-h). The quantitative measures for the 102 mm Abaqus simulations are also provided (i-l). Measurements of inward displacement were taken along the red line superimposed on each of the geometries starting at the base. Experimental blue light measurements are plotted in black and the measurements taken from the FEA results are plotted in red (Color figure online)

**Table 4 Comparison of qualitative agreement for individual components**

Article	Qualitative Agreement	Scale Factor	OffsetRequired	BL Confidence
51 mm Walls in Ansys	Yes-High	0.7	0	High
51 mm Roof in Ansys	Yes-Medium	1	0.03	Med
51 mm House in Ansys	Yes-High	1	0.03	High
102 mm Walls in Ansys	Yes-Medium	0.5	0.02	Low
102 mm Roof in Ansys	Yes-Medium	1	0	Low
102 mm House in Ansys	Yes-High	1	0	High
102 mm House in Abaqus	Yes-High	1	0.03	Low
102 mm Roof in Abaqus	Yes-Medium	0.5	0	Low
102 mm House in Abaqus	Yes-High	2	0	High

Overall, the CL articles are in a final state where some stresses are relaxed and result in part distortion within this method of analysis. However, these stresses manifest themselves completely in distortion, leaving only minimal residual stress in the CL features; this means that some distortions may be lost in the superposition method, resulting in the observed reduced accuracy, particularly in areas near the Roof/Wall interface.

Lastly, the distortions for the full house assembly and superposition features appear to show reduced error as compared to the individual components. This may be due to the differences in scales for the individual components versus the assemblies. For the individual components, maximum displacements are typically between 0.05 and 0.08 mm for individual components, while maximum displacements are between 0.1 and 0.5 mm for assemblies. Therefore, since the error for individual components is on the order of the layer thickness, small deviations in displacement may approach the 25  $\mu\text{m}$  limit of blue light scanning equipment and the graph might simply be plotting noise from the scanner or inexact geometric build rather than actual deviation due to stress buildup within the structure. This motivates follow-up analysis to determine the exact reason for the deviation in quantitative results with more accurate methods such as white light scanners that can achieve accuracies of a few microns.

### 4.3 Extensions of Superposition Approach for Different BCs

In the results presented up to this point, the superposition geometries (51mm and 102mm) possessed components that were tied together in the build direction. However, it may be necessary to utilize the proposed superposition method for CL geometries that exist in the transverse plane or even planes with normal directions non-orthogonal to the build direction. Therefore, two 51mm wall components were taken from the CL to construct a part made from the two boxes tied together side by side. As before, the full assembly was run in Ansys to compare against the superposition approach. The deformation observed in the full simulation of the side by side box, or 'double-box' geometry can be observed in Fig. 7(a). The patterns of deformation observed resemble those shown in Fig 2(d). The major difference being much less deformation observed along the interface between the two boxes due to

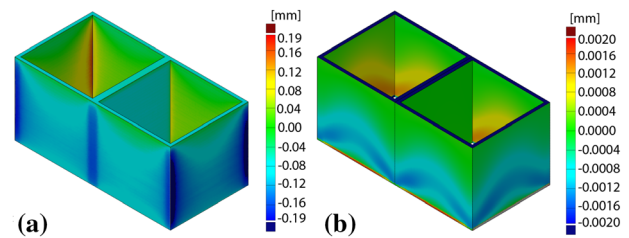


**Fig. 7** (a) Full house Ansys simulation of the double box geometry. (b) Ansys superposition simulation of the double box geometry

the increased thickness of the wall at the interface. For most of the double box structure, the full simulation result looks quite similar to the single box result, all except the central wall which shows slight shrinkage. The displacement appears to be about 0.08 mm on each side, which represents about 4% shrinkage on 1/2 of the 4 mm wall. Thermal shrinkage (perhaps combined with solidification) appears to be a simple explanation of that result.

The Ansys superposition simulation results are presented in Fig. 7(b). Overall, there exists a significant deviation from the full simulation result presented in Fig. 7(a). While the full simulation possesses a continuous evolution of the deformation along the faces of the box, the superposition deformation takes the shape of a u-shaped band that runs along each of the faces. Additionally, the magnitude of the distortion is very low relative to the full simulation. While this drop off in distortion was observed in all super position simulations, the simulation result presented in 7b only possesses a few microns of distortion. Although the full simulation on a single box might be expected to show something similar to the superposition result, it appears that each box is simulated to mostly shrink on the outside with little motion on the inside. This is apparent in Fig 2(b) (full Ansys simulation of a box) which is green on the inside of each face/wall but light blue on the outside. When the two boxes are conjoined, Fig 7(b), the equilibration of the two boxes makes only negligible difference to the central wall. The superposed double box result is less like the full simulation than for the Walls + Roof combination but understanding it in detail would require comparing the stress states along with the

distortions in the separated condition to check that the equilibration step (in superposition) is leading to logical results. The discrepancies between the full house assembly (Fig. 7a) and superposition (7b) may be due to the major variable being passed to the superposition result which is the residual stress left over from the simulation of the 51mm walls component that makes up this assembly. Clearly, the small amount of distortion present in Fig. 7(b) illustrates that only a small amount of residual stress is passed to the superposition assembly. The ability of the 51mm box component to relieve the majority of the stress it experiences during the simulated building process though distortion means that less residual stress is able to be passed onto the superposition simulation. The only area where residual stress from the component is being passed is along the band of distortion observed in Fig 7(b). In both Figs. 7(a) and 3(d) (102 mm Ansys walls component) a region of a small amount of distortion can be observed above a semi-circle of no distortion that interacts with the baseplate. In these regions, the proximity to the baseplate prevents the full relief of the residual stress via strain. This means that residual stress is built up in this region to be passed on into the superposition simulation, resulting in the band of distortion apparent in Fig. 7(b).

Although experimental results are necessary to validate the full- and superposition simulations, the results above illustrate that superposition approach, in its current form, is less effective when the majority of stresses built up during the key CL feature simulation areas are relieved via distortion and an assembly of the CL features superimposes these regions. This is especially obvious in this test case due to the boundary condition imposed here. The interface between the roof and the walls for the house assembly superimposes regions of relatively residual stresses in the component features and, therefore, better matches the full simulation results. Understanding of how individual components relieve stress during the simulated build process and which regions of individual parts are able to fully, or nearly fully, relieve residual stress can improve implementation of this technique. Work is ongoing to measure the stress present in the experimental parts to compare to the simulation results and inform optimization of component library development.

## 5. Conclusion

We investigated L-PBF AM shapes as potential entries within a component library (CL) of geometric features to enable fast predictions of component-level distortion. Experimental blue light and commercial FEA modeling were used to compare the distortion values within individual shapes and their combinations. As a whole, good qualitative results were observed between simulations and blue light data. The following conclusions can be made:

- The 102 mm parts with 1 mm wall thickness showed the most distortion. This points to the idea that larger, thinner metal AM components tend to relieve thermal gradients through displacement/distortion (as compared to residual stress buildup).
- Overall, the qualitative profiles did not change much with scaling of size or wall thickness.
- Abaqus and Ansys both perform similarly in qualitative and quantitative comparisons. Abaqus tended to better capture qualitative profiles seen near the baseplate whereas

Ansys appeared to be quantitatively closer to observed peak deviations on a number of articles.

- The use of CLs resulted in over 20-times savings in computational cost while reproducing overall trends in distortion for test geometry assemblies. However, more analysis is necessary to determine which shapes and geometries are best suited as CL features, particularly for larger parts and parts with substantial thickness, curved members, and/or more than two components.
- Stress relief via distortion in the simulation of the individual components results in less residual stress being passed onto the superposition assemblies to use to approximate distortion. This resulted in a drop in magnitude of the house assembly distortions and an inaccurate prediction of distortion for the side-by-side box simulations. Care should be taken to consider the residual stress state of the individual components in the component library when implementing the superposition method described in this manuscript.

Therefore, it is anticipated that the use of CLs for L-PBF AM geometries have great potential to facilitate efficient simulations of the distortions within full component AM assemblies. Future investigations involving the evaluation of the residual stress distributions within CLs are necessary and are forthcoming.

## Acknowledgments

This work was funded by the Department of Energy's Kansas City National Security Campus (KCNSC) which is operated and managed by Honeywell Federal Manufacturing Technologies, LLC under contract number DE-NA0002839. JVG, JGP, MF, JZ, MB & ADR are grateful for support from the KCNSC under contract number N000334546.

### Funding

This work was funded by the Department of Energy's Kansas City National Security Campus (KCNSC) which is operated and managed by Honeywell Federal Manufacturing Technologies, LLC under contract number DE-NA0002839.

## References

1. A. Riemer, S. Leuders, M. Thöne, H.A. Richard, T. Tröster and T. Niendorf, On the Fatigue Crack Growth Behavior in 316L Stainless Steel Manufactured by Selective Laser Melting, *Eng. Fract. Mech.*, 2014, **120**, p 15–25
2. J.P. Kruth, J. Deckers, E. Yasa and R. Wauthlé, Assessing and Comparing Influencing Factors of Residual Stresses in Selective Laser Melting Using a Novel Analysis Method, *Proc. Inst. Mech. Eng. Part B J. Eng. Manuf.*, 2012, **226**, p 980–991
3. A.S. Wu, D.W. Brown, M. Kumar, G.F. Gallegos and W.E. King, An Experimental Investigation into Additive Manufacturing-Induced Residual Stresses in 316L Stainless Steel, *Metall. Mater. Trans. A Phys. Metall. Mater. Sci.*, 2014, **45**, p 6260–6270
4. F. Neugebauer, N. Keller, V. Ploshikhin, F. Feuerhahn, H. Köhler, Multi Scale FEM Simulation for Distortion Calculation in Additive Manufacturing of Hardening Stainless Steel, *Proc. Int. Work. Therm. Form. Weld. Distortion.* (2014) 1–11
5. N.E. Hodge, R.M. Ferencz and R.M. Vignes, Experimental Comparison of Residual Stresses for a Thermomechanical Model for the Simulation of Selective Laser Melting, *Addit. Manuf.*, 2016, **12**, p 159–168
6. M. Ghasri-Khouzani, H. Peng, R. Rogge, R. Attardo, P. Ostiguy, J. Neidig, R. Billo, D. Hoelzle and M.R. Shankar, Experimental Measurement of Residual Stress and Distortion in Additively Manu-

- factured Stainless Steel Components with Various Dimensions, *Mater. Sci. Eng. A.*, 2017, **707**, p 689–700
7. T. Simson, A. Emmel, A. Dwars and J. Böhm, Residual Stress Measurements on AISI 316L Samples Manufactured by Selective Laser Melting, *Addit. Manuf.*, 2017, **17**, p 183–189
  8. T. Mukherjee, W. Zhang and T. DebRoy, An Improved Prediction of Residual Stresses and Distortion in Additive Manufacturing, *Comput. Mater. Sci.*, 2017, **126**, p 360–372
  9. C. Li, Z.Y. Liu, X.Y. Fang and Y.B. Guo, On the Simulation Scalability of Predicting Residual Stress and Distortion in Selective Laser Melting, *J. Manuf. Sci. Eng.*, 2018, **140**, p 041013
  10. R.J. Williams, C.M. Davies and P.A. Hooper, A Pragmatic Part Scale Model for Residual Stress and Distortion Prediction in Powder Bed Fusion, *Addit. Manuf.*, 2018, **22**, p 416–425
  11. M. Strantza, R.K. Ganeriwala, B. Clausen, T.Q. Phan, L.E. Levine, D. Pagan, W.E. King, N.E. Hodge and D.W. Brown, Coupled Experimental and Computational Study of Residual Stresses in Additively Manufactured Ti-6Al-4V Components, *Mater. Lett.*, 2018, **231**, p 221–224
  12. R.K. Ganeriwala, M. Strantza, W.E. King, B. Clausen, T.Q. Phan, L.E. Levine, D.W. Brown and N.E. Hodge, Evaluation of a Thermomechanical Model for Prediction of Residualstress During Laser Powder Bed Fusion of Ti-6Al-4V, *Addit. Manuf.*, 2019, **27**, p 489–502
  13. K. An, L. Yuan, L. Dial, I. Spinelli, A.D. Stoica and Y. Gao, Neutron Residual Stress Measurement and Numerical Modeling in a Curved Thin-Walled Structure by Laser Powder bed Fusion Additive Manufacturing, *Mater. Des.*, 2017, **135**, p 122–132
  14. B. Clausen, C.R. D’Elia, M.B. Prime, M.R. Hill, J.E. Bishop, K.L. Johnson, B.H. Jared, K.M. Allen, D.K. Balch, R.A. Roach, D.W. Brown, Complementary Measurements of Residual Stresses Before and After Base Plate Removal in an Intricate Additively-Manufactured Stainless-Steel Valve Housing, *Addit. Manuf.* 36 (2020)
  15. L. Zhang, B. Song, A. Zhao, R. Liu, L. Yang and Y. Shi, Study on Mechanical Properties of Honeycomb Pentamode Structures Fabricated by Laser Additive Manufacturing: Numerical Simulation and Experimental Verification, *Compos. Struct.*, 2019, **226**, p 111199
  16. Y. Zhang, D. Kong and S. Liu, Experimental Study of Forced Convection Heat Transfer of Graded Metal Honeycomb Fabricated by Additive Manufacturing, *Int. Commun. Heat Mass Transf.*, 2018, **98**, p 67–73
  17. S. Chekurov, J. Kajaste, K. Saari, H. Kauranne, M. Pietola and J. Partanen, Additively Manufactured High-Performance Counterflow Heat Exchanger, *Prog. Addit. Manuf.*, 2019, **4**, p 55–61
  18. S. Martínez-Pellitero, E. Cuesta, S. Giganto and J. Barreiro, New Procedure for Qualification of Structured Light 3D Scanners Using an Optical Feature-Based Gauge, *Opt. Lasers Eng.*, 2018, **110**, p 193–206
  19. S. Gao, Z. Tan, L. Lan and B. He, Effects of Geometrical Size and Structural Feature on the Shape-Distortion Behavior of Hollow Ti-Alloy Blade Fabricated by Additive Manufacturing Process, *J. Laser Appl.*, 2020, **32**, p 032005
  20. T. Mayer, G. Brändle, A. Schönenberger, R. Eberlein, Simulation and Validation of Residual Deformations in Additive Manufacturing of Metal Parts, *Heliyon*. 6 (2020)

**Publisher’s Note** Springer Nature remains neutral with regard to jurisdictional claims in published maps and institutional affiliations.